The multi-layered ring under parabolic distribution of radial stresses combined with uniform internal and external pressure

Christos F. Markides, Ermioni D. Pasiou, Stavros K. Kourkoulis
National Technical University of Athens, School of Applied Mathematical and Physical Sciences, Department of Mechanics,
5 Heroes of Polytechnion Avenue, Theocaris Bld., Zografou Campus, 157 73 Athens, Greece

ABSTRACT. A recently introduced solution for the stress- and displacement-fields, developed in a multi-layered circular ring, composed of a finite number of linearly elastic concentric layers, subjected to a parabolic distribution of radial stresses, is here extended to encompass a more general loading scheme, closer to actual conditions. The loading scheme includes, besides the parabolic radial stresses, a combination of uniform pressures acting along the outer- and inner-most boundaries of the layered ring. The analytic solution of the problem is achieved by adopting Savin's pioneering approach for an infinite plate with a hole strengthened by rings. Taking advantage of the results provided by the analytic solution, a numerical model, simulating the configuration of a three-layered ring (quite commonly encountered in practical applications) is validated. The numerical model is then used for a parametric analysis enlightening some crucial aspects of the overall response of the ring.

KEYWORDS. Multi-layered ring; Parabolic pressure; Stress and displacement fields; Uniform pressure; Complex potentials.

INTRODUCTION

In a recently published paper [1] the stress- and displacement-fields developed in a circular multi-layered ring were considered both analytically and numerically. The ring was composed by a finite number of concentric layers made of different linearly elastic materials and it was loaded by a parabolic distribution of radial stresses acting along two finite arcs of the outer boundary of the outer-most layer. In general, the configuration of multi-layered rings is common in quite a few engineering applications of increased interest, ranging from Biomechanics (human aorta) to Fluid Mechanics (insulated pipes). Such composite rings are usually loaded either by uniformly distributed internal or external pressure or by a combination of them.

In the study by Markides et al. [1] a more complicated loading scheme was considered consisting of radial stresses acting along two finite arcs of the external boundary of the outer-most layer (antisymmetric with respect to the geometric centre of the ring) distributed according to a parabolic law. Such a loading scheme appears in case a circular ring is compressed between either plane or curved jaws (as it is for example the jaws of the device introduced by the International Society for Rock Mechanics (ISRM) [2] for the standardized implementation of the Brazilian-disc test).

The solution by Markides et al. [1] is here generalized to confront a more general loading scheme including, besides the parabolic radial stresses, a combination of uniform pressures acting along the outer- and inner-most boundaries of the

layered ring. For the analytic solution of the problem, the procedure proposed by Savin [3] for an infinite plate with a hole strengthened by rings is adopted as it was done also in ref. [1]. The specific procedure is based on the complex potentials technique introduced by Muskhelishvili [4]. The analytic solution achieved provides full-field closed-form expressions for both the stresses and the displacements. However, the specific expressions, in spite of their "elegance" and their numerous advantages (related mainly to their generality and the fact that they are expandable to rings that are made up of any number of concentric layers), are somehow "lengthy" and cumbersome. As a result, detailed parametric analyses of the (quite a few) factors influencing the final outcomes become rather difficult.

To overcome the above mentioned difficulty, the problem is revisited, also, numerically using the Finite Element method and the commercially available software ANSYS. For the validation of the numerical model, the data obtained from the analytic solution for the case of a ring made up of three concentric layers are used. Then the validated numerical model is used for a parametric study of the role of some critical parameters (i.e., the elastic modulus and thickness of the intermediate layer and also the length of the arcs loaded by the parabolic distribution of radial stresses) on the overall stress- and displacement-fields developed in the ring.

THEORETICAL CONSIDERATIONS

The problem and the basic assumptions

Consider a multi-layered hollow cylinder of length w consisting of n concentric hollow cylinders of different thicknesses, perfectly joined together without any gaps at all. The cylinders are assumed to be made of homogeneous, isotropic and linearly elastic materials. The multi-layered cylinder as a whole is in equilibrium under the simultaneous action of three different kinds of loading: inner and outer uniform pressure all along its inner and outer lateral surfaces and a parabolic pressure acting along two finite parts of its outer periphery, antisymmetric with respect to the section's center. All three types of loading act in the body's normal cross-section and remain constant along its length. Ignoring its weight, stresses and displacements are to be determined at any point of the multi-layered cylinder. Clearly, the as above described configuration corresponds to a 1st fundamental problem of plane linear elasticity for the body's cross-section, i.e., the multi-layered circular ring. In this context, Muskhelishvili's method of complex potentials [4] will be employed for the analytic solution.

Mathematical formulation

Under the above assumptions, the multi-layered ring is considered lying in the $z=x+iy=re^{i\theta}$ complex plane, Fig.1. The origin of the Cartesian reference coincides with the center of the ring. The n constituent concentric rings are numbered in such a way so that they are encountered in the order 1, 2,…, n as one moves from the origin towards the outer perimeter of the multi-layered ring. The arbitrary ring is denoted by the index j ($1 \le j \le n$) and its boundaries are L_j and L_{j+1} corresponding to the radii $r=R_j$ and $r=R_{j+1}$ ($R_{j+1} > R_j$), respectively. In general, it holds that $(R_2-R_1) \ne (R_3-R_2) \ne \dots (R_{n+1}-R_n)$. Adjacent constituent rings are perfectly joined together along their common interfaces. The inner boundary of the innermost ring, L_1, for $r=R_1$, is subjected to a uniform pressure of magnitude $p_I>0$. The outer boundary of the outermost ring, L_{n+1}, for $r=R_{n+1}$, is under the simultaneous action of a uniform pressure of magnitude $p_E>0$ exerted all over L_{n+1}, and a parabolic pressure of magnitude $p(\theta)>0$ acting along two finite arcs of L_{n+1}, antisymmetric with respect to the ring's center. Each one of these arcs has a length equal to $2\omega_o R_{n+1}$, where ω_o corresponds to the half loaded rim. Particularly, $p(\theta)$ is here considered equal to:

$$p(\theta) = P_c \left[1 - \sin^2(\phi_o - \theta) / \sin^2 \omega_o \right], \qquad P_c \equiv \max\{p(\theta)\} = \frac{2F \sin^2 \omega_o}{R_{n+1}(\sin 2\omega_o - 2\omega_o \cos 2\omega_o)w} \qquad (1)$$

where ϕ_o is the arbitrary angle formed by the axis of symmetry of the parabolic pressure and x-axis (measured from x-axis in the anticlockwise direction) and F ($F>0$) is the resultant force due to $p(\theta)$. Obviously, for the as above described loading conditions, the multi-layered ring as a whole and each constituent j-ring separately, are in equilibrium and for that configuration the stress- and displacement-fields are to be determined for each j-ring.

According to Muskhelishvili, the latter can be implemented by obtaining on each j-ring two analytic functions of the complex variable z, the complex potentials $\varphi_j(z)$ and $\psi_j(z)$, in terms of which stresses and displacements are expressed as [4]:

$$\sigma_\theta^{(j)} + \sigma_r^{(j)} = 4\Re\left\{\varphi_j{}'(z)\right\} \tag{2}$$

$$\sigma_r^{(j)} - i\tau_{r\theta}^{(j)} = \varphi_j{}'(z) + \overline{\varphi_j{}'(z)} - e^{i2\theta}\left[\bar{z}\,\varphi_j{}''(z) + \psi_j{}'(z)\right] \tag{3}$$

$$u_r^{(j)} - iu_\theta^{(j)} = \frac{e^{i\theta}}{2\mu_j}\left[\kappa_j\,\overline{\varphi_j(z)} - \bar{z}\,\varphi_j{}'(z) - \psi_j(z)\right] \tag{4}$$
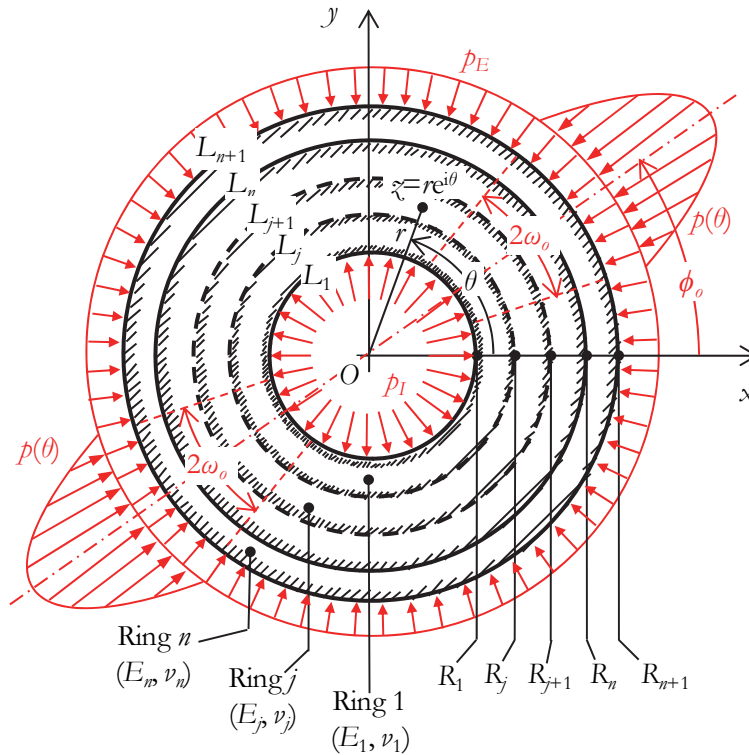

Figure 1: The configuration of the problem and definition of symbols.

In Eqs.(2-4) prime and double prime denote first and second derivative, bar denotes the complex conjugate and $\Re$ is the real part; in addition, μ_j denotes the shear modulus and $\varkappa_j$ is the Muskhelishvili's constant, equal to $3-4v_j$ or $(3-v_j)/(1+v_j)$, for plane strain or plane stress respectively, with v_j indicating the Poisson's ratio.

Regarding $\varphi_j(z)$ and $\psi_j(z)$, their analytic character on each *j*-circular ring permits representing them by Laurent series as:

$$\varphi_j(z) = \sum_{-\infty}^{+\infty} a_k^{(j)} z^k, \qquad \psi_j(z) = \sum_{-\infty}^{+\infty} b_k^{(j)} z^k, \qquad j = 1, 2, ..., n \tag{5}$$

Therefore the problem reduces to the determination of the coefficients $a_k^{(j)}$ and $b_k^{(j)}$, a task that will be achieved by fulfilling the boundary conditions of the problem. Before implementing this step, however, it is to be mentioned that it is not possible to obtain directly all $a_k^{(j)}$ and $b_k^{(j)}$; namely, for a 1st fundamental problem $\varphi_j(z)$ is determined apart from an arbitrary complex constant and an arbitrary real constant C appearing in a term of the form iCz. In this context, $a_0^{(j)}$ and the imaginary part, $\Im\left\{a_1^{(j)}\right\}$, of the coefficient $a_1^{(j)}$ remain arbitrary. In the particular problem studied, both are set equal to zero for convenience. What is more, $\psi_j(z)$ is obtained apart from an arbitrary complex constant so $b_0^{(j)}$ remains arbitrary. Actually, it can be seen that for the present problem only one out of all $b_0^{(j)}$ can be arbitrarily fixed while the remaining ones are

subjected to determination. Here it is assumed that $b_0^{(1)} = 0$. It is only under these simplifying assumptions that the remaining coefficients $a_k^{(j)}$ and $b_k^{(j)}$ can be determined with the aid of the boundary conditions of the problem. These conditions are classified into two categories:

i. The boundary values of stresses on the multi-layered ring's boundaries as a whole, reading as:

$$\sigma_r^{(1)} = -p_I, \quad \tau_{r\theta}^{(1)} = 0, \qquad \qquad \text{for } r = R_1 \quad \text{and} \quad 0 \le \theta \le 2\pi \qquad (6)$$

$$\sigma_r^{(n+1)} = -p_E - p(\theta), \tau_{r\theta}^{(n+1)} = 0, \qquad \text{for } r = R_{n+1} \text{ and}$$

$$\phi_o - \omega_o \le \theta \le \phi_o + \omega_o \ \cup \ \pi + \phi_o - \omega_o \le \theta \le \pi + \phi_o + \omega_o \qquad (7)$$

$$\sigma_r^{(n+1)} = -p_E, \quad \tau_{r\theta}^{(n+1)} = 0, \qquad \qquad \text{for } r = R_{n+1} \text{ and}$$

$$\phi_o + \omega_o \le \theta \le \pi + \phi_o - \omega_o \cup \pi + \phi_o + \omega_o \le \theta \le 2\pi + \phi_o - \omega_o \qquad (8)$$

ii. The values of stresses and displacements along the interfaces L_{j+1}, $j=1,\ldots,n-1$, between the j- and $(j+1)$-ring, due to their firmly joining, reading as:

$$\sigma_r^{(j)} = \sigma_r^{(j+1)}, \quad \tau_{r\theta}^{(j)} = \tau_{r\theta}^{(j+1)}, \qquad \text{for } r = R_{j+1} \text{ and } 0 \le \theta \le 2\pi, \qquad (9)$$

$$u_r^{(j)} = u_r^{(j+1)}, \quad u_\theta^{(j)} = u_\theta^{(j+1)}, \qquad \text{for } r = R_{j+1} \text{ and } 0 \le \theta \le 2\pi \qquad (10)$$

Combining Eqs.(3-10) and comparing terms of $e^{ik\theta}$ of the same k-order, in the expressions resulting, the following equations are obtained involving $a_k^{(j)}$ and $b_k^{(j)}$:

Due to the condition of uniform pressure on L_1:

$$2\alpha_1^{(1)} + R_1^{-2}\overline{b}_{-1}^{(1)} = -p_I$$
$$R_1 a_2^{(1)} + R_1^{-3}\overline{b}_{-2}^{(1)} = 0$$
$$3R_1^2 a_3^{(1)} + R_1^{-2}\overline{a}_{-1}^{(1)} + b_1^{(1)} = 0$$
$$R_1^2 a_3^{(1)} - R_1^{-2}\overline{a}_{-1}^{(1)} + R_1^{-4}\overline{b}_{-3}^{(1)} = 0 \qquad (11)$$

$$\left. \begin{array}{l} kR_1^{k-1} a_k^{(1)} + R_1^{-(k-1)}\overline{a}_{-(k-2)}^{(1)} + R_1^{k-3} b_{k-2}^{(1)} = 0 \\ R_1^{k-1} a_k^{(1)} - (k-2)R_1^{-(k-1)}\overline{a}_{-(k-2)}^{(1)} + R_1^{-(k+1)}\overline{b}_{-k}^{(1)} = 0 \end{array} \right\}, \qquad (k = 4,5,\ldots)$$

where $\alpha_1^{(1)}$ is the real part of $a_1^{(1)}$.

Due to the condition of uniform and parabolic pressure on L_{n+1}, (after the factor $p(\theta)$, appearing in the first of Eqs.(1) has been expanded in Fourier series):

$$2\alpha_1^{(n)} + R_{n+1}^{-2}\overline{b}_{-1}^{(n)} = -p_E - \frac{P_c}{\pi}\left(2\omega_o - \frac{2\omega_o - \sin 2\omega_o}{2\sin^2 \omega_o}\right)$$

$$R_{n+1} a_2^{(n)} + R_{n+1}^{-3}\overline{b}_{-2}^{(n)} = 0$$

$$3R_{n+1}^2 a_3^{(n)} + R_{n+1}^{-2}\overline{a}_{-1}^{(n)} + b_1^{(n)} = \frac{P_c}{\pi}\left[\sin 2\omega_o - \frac{1}{2\sin^2\omega_o}\left(\sin 2\omega_o - \omega_o - \frac{\sin 2\omega_o \cos 2\omega_o}{2}\right)\right]e^{-i2\phi_o}$$

$$R_{n+1}^2 a_3^{(n)} - R_{n+1}^{-2}\overline{a}_{-1}^{(n)} + R_{n+1}^{-4}\overline{b}_{-3}^{(n)} = \frac{-P_c}{3\pi}\left[\sin 2\omega_o - \frac{1}{2\sin^2\omega_o}\left(\sin 2\omega_o - \omega_o - \frac{\sin 2\omega_o \cos 2\omega_o}{2}\right)\right]e^{-i2\phi_o}$$

$$(k-2)\left(kR_{n+1}^{k-1}a_k^{(n)} + R_{n+1}^{-(k-1)}\overline{a}_{-(k-2)}^{(n)} + R_{n+1}^{k-3}b_{k-2}^{(n)}\right) = \frac{P_c}{\pi}\left\{\frac{\sin(k-1)\omega_o}{k-1} - \frac{1}{2\sin^2\omega_o}\left[\frac{\sin(k-1)\omega_o}{k-1}\right.\right.$$

$$\left.\left. + \frac{(k-1)\cos 2\omega_o \sin(k-1)\omega_o - 2\sin 2\omega_o \cos(k-1)\omega_o}{4-(k-1)^2}\right]\right\}\left(1-e^{-ik\pi}\right)e^{-i(k-1)\phi_o}, \qquad (k=4,5,...)$$

$$k\left[R_{n+1}^{k-1}a_k^{(n)} - (k-2)R_{n+1}^{-(k-1)}\overline{a}_{-(k-2)}^{(n)} + R_{n+1}^{-(k+1)}\overline{b}_{-k}^{(n)}\right] = \frac{-P_c}{\pi}\left\{\frac{\sin(k-1)\omega_o}{k-1} - \frac{1}{2\sin^2\omega_o}\left[\frac{\sin(k-1)\omega_o}{k-1}\right.\right.$$

$$\left.\left. + \frac{(k-1)\cos 2\omega_o \sin(k-1)\omega_o - 2\sin 2\omega_o \cos(k-1)\omega_o}{4-(k-1)^2}\right]\right\}\left(1-e^{-ik\pi}\right)e^{-i(k-1)\phi_o}, \qquad (k=4,5,...) \qquad (12)$$

where $\alpha_1^{(n)}$ is the real part of $a_1^{(n)}$.

<u>Due to the condition for equal action-reaction at facing points of the *j*- and (*j*+1)-ring, because of perfect matching of the layers:</u>

$$2\alpha_1^{(j)} + R_{j+1}^{-2}\overline{b}_{-1}^{(j)} - 2\alpha_1^{(j+1)} - R_{j+1}^{-2}\overline{b}_{-1}^{(j+1)} = 0$$

$$R_{j+1}a_2^{(j)} + R_{j+1}^{-3}\overline{b}_{-2}^{(j)} - R_{j+1}a_2^{(j+1)} - R_{j+1}^{-3}\overline{b}_{-2}^{(j+1)} = 0$$

$$3R_{j+1}^2 a_3^{(j)} + R_{j+1}^{-2}\overline{a}_{-1}^{(j)} + b_1^{(j)} - 3R_{j+1}^2 a_3^{(j+1)} - R_{j+1}^{-2}\overline{a}_{-1}^{(j+1)} - b_1^{(j+1)} = 0$$

$$R_{j+1}^2 a_3^{(j)} - R_{j+1}^{-2}\overline{a}_{-1}^{(j)} + R_{j+1}^{-4}\overline{b}_{-3}^{(j)} - R_{j+1}^2 a_3^{(j+1)} + R_{j+1}^{-2}\overline{a}_{-1}^{(j+1)} - R_{j+1}^{-4}\overline{b}_{-3}^{(j+1)} = 0 \quad \left(j=1,2,...,n-1\right)$$

$$\left.\begin{array}{l} kR_{j+1}^{k-1}a_k^{(j)} + R_{j+1}^{-(k-1)}\overline{a}_{-(k-2)}^{(j)} + R_{j+1}^{k-3}b_{k-2}^{(j)} \\ \quad - kR_{j+1}^{k-1}a_k^{(j+1)} - R_{j+1}^{-(k-1)}\overline{a}_{-(k-2)}^{(j+1)} - R_{j+1}^{k-3}b_{k-2}^{(j+1)} = 0 \\ \\ R_{j+1}^{k-1}a_k^{(j)} - (k-2)R_{j+1}^{-(k-1)}\overline{a}_{-(k-2)}^{(j)} + R_{j+1}^{-(k+1)}\overline{b}_{-k}^{(j)} \\ \quad - R_{j+1}^{k-1}a_k^{(j+1)} + (k-2)R_{j+1}^{-(k-1)}\overline{a}_{-(k-2)}^{(j+1)} - R_{j+1}^{-(k+1)}\overline{b}_{-k}^{(j+1)} = 0 \end{array}\right\}, \; \left(k=4,5,...\right) \qquad (13)$$

where $\alpha_1^{(j)}$ is the real part of $a_1^{(j)}$.

<u>Due to the condition for the same displacements of facing points of the *j*- and (*j*+1)-ring, because of perfect matching of the layers:</u>

$$2\frac{\mu_2}{\mu_1}R_2^2 a_2^{(1)} - b_0^{(2)} - 2R_2^2 a_2^{(2)} = 0$$

$$\frac{\mu_{j+1}}{\mu_j}\left(b_0^{(j)} + 2R_{j+1}^2 a_2^{(j)}\right) - b_0^{(j+1)} - 2R_{j+1}^2 a_2^{(j+1)} = 0, \qquad \left(j = 2,3,...,n-1\right)$$

$$\left.\begin{array}{l} \dfrac{\mu_{j+1}}{\mu_j}\left[\left(\kappa_j - 1\right)R_{j+1}\alpha_1^{(j)} - R_{j+1}^{-1}\overline{b}_{-1}^{(j)}\right] - \left(\kappa_{j+1} - 1\right)R_{j+1}\alpha_1^{(j+1)} + R_{j+1}^{-1}\overline{b}_{-1}^{(j+1)} = 0 \\[2em] \dfrac{\mu_{j+1}}{\mu_j}\left(\kappa_j R_{j+1}^2 a_2^{(j)} - R_{j+1}^{-2}\overline{b}_{-2}^{(j)}\right) - \kappa_{j+1}R_{j+1}^2 a_2^{(j+1)} + R_{j+1}^{-2}\overline{b}_{-2}^{(j+1)} = 0 \\[2em] \dfrac{\mu_{j+1}}{\mu_j}\left(3R_{j+1}^3 a_3^{(j)} - \kappa_j R_{j+1}^{-1}\overline{a}_{-1}^{(j)} + R_{j+1}b_1^{(j)}\right) - 3R_{j+1}^3 a_3^{(j+1)} + \kappa_{j+1}R_{j+1}^{-1}\overline{a}_{-1}^{(j+1)} - R_{j+1}b_1^{(j+1)} = 0 \\[2em] \dfrac{\mu_{j+1}}{\mu_j}\left(\kappa_j R_{j+1}^3 a_3^{(j)} + R_{j+1}^{-1}\overline{a}_{-1}^{(j)} - R_{j+1}^{-3}\overline{b}_{-3}^{(j)}\right) - \kappa_{j+1}R_{j+1}^3 a_3^{(j+1)} - R_{j+1}^{-1}\overline{a}_{-1}^{(j+1)} + R_{j+1}^{-3}\overline{b}_{-3}^{(j+1)} = 0 \\[3em] \left.\begin{array}{l}\dfrac{\mu_{j+1}}{\mu_j}\left(kR_{j+1}^k a_k^{(j)} - \kappa_j R_{j+1}^{-(k-2)}\overline{a}_{-(k-2)}^{(j)} + R_{j+1}^{k-2}b_{k-2}^{(j)}\right) \\[1.5em] \qquad - kR_{j+1}^k a_k^{(j+1)} + \kappa_{j+1}R_{j+1}^{-(k-2)}\overline{a}_{-(k-2)}^{(j+1)} - R_{j+1}^{k-2}b_{k-2}^{(j+1)} = 0 \\[2em] \dfrac{\mu_{j+1}}{\mu_j}\left[\kappa_j R_{j+1}^k a_k^{(j)} + \left(k-2\right)R_{j+1}^{-(k-2)}\overline{a}_{-(k-2)}^{(j)} - R_{j+1}^{-k}\overline{b}_{-k}^{(j)}\right] \\[1.5em] \qquad - \kappa_{j+1}R_{j+1}^k a_k^{(j+1)} - \left(k-2\right)R_{j+1}^{-(k-2)}\overline{a}_{-(k-2)}^{(j+1)} + R_{j+1}^{-k}\overline{b}_{-k}^{(j+1)} = 0\end{array}\right\}, \left(k = 4,5,...\right) \end{array}\right\} \begin{array}{l} (14) \\[6em] \left(j = 1,2,...,n-1\right) \end{array}$$

Properly rearrangement of Eqs.(11-14), yields the following linear systems of equations for the determination of $a_k^{(j)}$ and $b_k^{(j)}$, for any specific number n of constituent rings:

$$2\alpha_1^{(1)} + R_1^{-2}\overline{b}_{-1}^{(1)} = -p_I$$

$$2\alpha_1^{(n)} + R_{n+1}^{-2}\overline{b}_{-1}^{(n)} = -p_E - \frac{P_c}{\pi}\left(2\omega_o - \frac{2\omega_o - \sin 2\omega_o}{2\sin^2\omega_o}\right) \tag{15}$$

$$\left.\begin{array}{l} 2\alpha_1^{(j)} + R_{j+1}^{-2}\overline{b}_{-1}^{(j)} - 2\alpha_1^{(j+1)} - R_{j+1}^{-2}\overline{b}_{-1}^{(j+1)} = 0 \\[1.5em] \dfrac{\mu_{j+1}}{\mu_j}\left[\left(\kappa_j - 1\right)R_{j+1}\alpha_1^{(j)} - R_{j+1}^{-1}\overline{b}_{-1}^{(j)}\right] - \left(\kappa_{j+1} - 1\right)R_{j+1}\alpha_1^{(j+1)} + R_{j+1}^{-1}\overline{b}_{-1}^{(j+1)} = 0 \end{array}\right\}, \left(j = 1,2,...,n-1\right)$$

$$2\frac{\mu_2}{\mu_1}R_2^2 a_2^{(1)} - b_0^{(2)} - 2R_2^2 a_2^{(2)} = 0$$

$$\frac{\mu_{j+1}}{\mu_j}\left(b_0^{(j)} + 2R_{j+1}^2 a_2^{(j)}\right) - b_0^{(j+1)} - 2R_{j+1}^2 a_2^{(j+1)} = 0, \qquad \left(j = 2,3,...,n-1\right)$$

$$R_1 a_2^{(1)} + R_1^{-3}\overline{b}_{-2}^{(1)} = 0$$

$$R_{n+1} a_2^{(n)} + R_{n+1}^{-3}\overline{b}_{-2}^{(n)} = 0$$

$$\left.\begin{array}{c} R_{j+1} a_2^{(j)} + R_{j+1}^{-3}\overline{b}_{-2}^{(j)} - R_{j+1} a_2^{(j+1)} - R_{j+1}^{-3}\overline{b}_{-2}^{(j+1)} = 0 \\[2em] \dfrac{\mu_{j+1}}{\mu_j}\left(\kappa_j R_{j+1}^2 a_2^{(j)} - R_{j+1}^{-2}\overline{b}_{-2}^{(j)}\right) - \kappa_{j+1}R_{j+1}^2 a_2^{(j+1)} + R_{j+1}^{-2}\overline{b}_{-2}^{(j+1)} = 0 \end{array}\right\}, \; \left(j = 1,2,...,n-1\right) \tag{16}$$

(where, obviously, all coefficients appearing in Eqs.(16) are zero)

$$3R_1^2 a_3^{(1)} + R_1^{-2}\overline{a}_{-1}^{(1)} + b_1^{(1)} = 0$$

$$R_1^2 a_3^{(1)} - R_1^{-2}\overline{a}_{-1}^{(1)} + R_1^{-4}\overline{b}_{-3}^{(1)} = 0$$

$$3R_{n+1}^2 a_3^{(n)} + R_{n+1}^{-2}\overline{a}_{-1}^{(n)} + b_1^{(n)} = \frac{P_c}{\pi}\left[\sin 2\omega_o - \frac{1}{2\sin^2 \omega_o}\left(\sin 2\omega_o - \omega_o - \frac{\sin 2\omega_o \cos 2\omega_o}{2}\right)\right]e^{-i2\phi_o}$$

$$R_{n+1}^2 a_3^{(n)} - R_{n+1}^{-2}\overline{a}_{-1}^{(n)} + R_{n+1}^{-4}\overline{b}_{-3}^{(n)} = \frac{-P_c}{3\pi}\left[\sin 2\omega_o - \frac{1}{2\sin^2 \omega_o}\left(\sin 2\omega_o - \omega_o - \frac{\sin 2\omega_o \cos 2\omega_o}{2}\right)\right]e^{-i2\phi_o}$$

$$\left.\begin{array}{c} 3R_{j+1}^2 a_3^{(j)} + R_{j+1}^{-2}\overline{a}_{-1}^{(j)} + b_1^{(j)} - 3R_{j+1}^2 a_3^{(j+1)} - R_{j+1}^{-2}\overline{a}_{-1}^{(j+1)} - b_1^{(j+1)} = 0 \\[1.5em] R_{j+1}^2 a_3^{(j)} - R_{j+1}^{-2}\overline{a}_{-1}^{(j)} + R_{j+1}^{-4}\overline{b}_{-3}^{(j)} - R_{j+1}^2 a_3^{(j+1)} + R_{j+1}^{-2}\overline{a}_{-1}^{(j+1)} - R_{j+1}^{-4}\overline{b}_{-3}^{(j+1)} = 0 \\[1.5em] \dfrac{\mu_{j+1}}{\mu_j}\left(3R_{j+1}^3 a_3^{(j)} - \kappa_j R_{j+1}^{-1}\overline{a}_{-1}^{(j)} + R_{j+1}b_1^{(j)}\right) - 3R_{j+1}^3 a_3^{(j+1)} + \kappa_{j+1}R_{j+1}^{-1}\overline{a}_{-1}^{(j+1)} - R_{j+1}b_1^{(j+1)} = 0 \\[1.5em] \dfrac{\mu_{j+1}}{\mu_j}\left(\kappa_j R_{j+1}^3 a_3^{(j)} + R_{j+1}^{-1}\overline{a}_{-1}^{(j)} - R_{j+1}^{-3}\overline{b}_{-3}^{(j)}\right) - \kappa_{j+1}R_{j+1}^3 a_3^{(j+1)} - R_{j+1}^{-1}\overline{a}_{-1}^{(j+1)} + R_{j+1}^{-3}\overline{b}_{-3}^{(j+1)} = 0 \end{array}\right\}, \left(j = 1,2,...,n-1\right) \tag{17}$$

$$kR_1^{k-1}a_k^{(1)} + R_1^{-(k-1)}\overline{a}_{-(k-2)}^{(1)} + R_1^{k-3}b_{k-2}^{(1)} = 0$$

$$R_1^{k-1}a_k^{(1)} - (k-2)R_1^{-(k-1)}\overline{a}_{-(k-2)}^{(1)} + R_1^{-(k+1)}\overline{b}_{-k}^{(1)} = 0, \qquad \big(k = 4,5,...\big)$$

$$(k-2)\Big(kR_{n+1}^{k-1}a_k^{(n)} + R_{n+1}^{-(k-1)}\overline{a}_{-(k-2)}^{(n)} + R_{n+1}^{k-3}b_{k-2}^{(n)}\Big) = \frac{P_c}{\pi}\left\{\frac{\sin(k-1)\omega_o}{k-1} - \frac{1}{2\sin^2\omega_o}\left[\frac{\sin(k-1)\omega_o}{k-1}\right.\right.$$

$$\left.\left. + \frac{(k-1)\cos 2\omega_o \sin(k-1)\omega_o - 2\sin 2\omega_o \cos(k-1)\omega_o}{4-(k-1)^2}\right]\right\}\big(1 - e^{-ik\pi}\big)e^{-i(k-1)\phi_o}$$

$$k\left[R_{n+1}^{k-1}a_k^{(n)} - (k-2)R_{n+1}^{-(k-1)}\overline{a}_{-(k-2)}^{(n)} + R_{n+1}^{-(k+1)}\overline{b}_{-k}^{(n)}\right] = \frac{-P_c}{\pi}\left\{\frac{\sin(k-1)\omega_o}{k-1} - \frac{1}{2\sin^2\omega_o}\left[\frac{\sin(k-1)\omega_o}{k-1}\right.\right.$$

$$\left.\left. + \frac{(k-1)\cos 2\omega_o \sin(k-1)\omega_o - 2\sin 2\omega_o \cos(k-1)\omega_o}{4-(k-1)^2}\right]\right\}\big(1 - e^{-ik\pi}\big)e^{-i(k-1)\phi_o}$$

$$\left.\begin{aligned}
&kR_{j+1}^{k-1}a_k^{(j)} + R_{j+1}^{-(k-1)}\overline{a}_{-(k-2)}^{(j)} + R_{j+1}^{k-3}b_{k-2}^{(j)}\\
&\qquad - kR_{j+1}^{k-1}a_k^{(j+1)} - R_{j+1}^{-(k-1)}\overline{a}_{-(k-2)}^{(j+1)} - R_{j+1}^{k-3}b_{k-2}^{(j+1)} = 0\\[4pt]
&R_{j+1}^{k-1}a_k^{(j)} - (k-2)R_{j+1}^{-(k-1)}\overline{a}_{-(k-2)}^{(j)} + R_{j+1}^{-(k+1)}\overline{b}_{-k}^{(j)}\\
&\qquad - R_{j+1}^{k-1}a_k^{(j+1)} + (k-2)R_{j+1}^{-(k-1)}\overline{a}_{-(k-2)}^{(j+1)} - R_{j+1}^{-(k+1)}\overline{b}_{-k}^{(j+1)} = 0\\[4pt]
&\frac{\mu_{j+1}}{\mu_j}\Big(kR_{j+1}^k a_k^{(j)} - \kappa_j R_{j+1}^{-(k-2)}\overline{a}_{-(k-2)}^{(j)} + R_{j+1}^{k-2}b_{k-2}^{(j)}\Big)\\
&\qquad - kR_{j+1}^k a_k^{(j+1)} + \kappa_{j+1}R_{j+1}^{-(k-2)}\overline{a}_{-(k-2)}^{(j+1)} - R_{j+1}^{k-2}b_{k-2}^{(j+1)} = 0\\[4pt]
&\frac{\mu_{j+1}}{\mu_j}\left[\kappa_j R_{j+1}^k a_k^{(j)} + (k-2)R_{j+1}^{-(k-2)}\overline{a}_{-(k-2)}^{(j)} - R_{j+1}^{-k}\overline{b}_{-k}^{(j)}\right]\\
&\qquad - \kappa_{j+1}R_{j+1}^k a_k^{(j+1)} - (k-2)R_{j+1}^{-(k-2)}\overline{a}_{-(k-2)}^{(j+1)} + R_{j+1}^{-k}\overline{b}_{-k}^{(j+1)} = 0
\end{aligned}\right\}, (j = 1,2,...,n-1) \qquad (18)$$

$$\big(k = 4,5,...\big)$$

For the $13n-1$ unknowns appearing in Eqs.(15-18), i.e., for $\left\{\alpha_1^{(1)},\alpha_1^{(2)},...,\alpha_1^{(n)}\right\}$, $\left\{a_2^{(1)},a_2^{(2)},...,a_2^{(n)}\right\}$, $\left\{a_3^{(1)},a_3^{(2)},...,a_3^{(n)}\right\}$, $\left\{\overline{a}_{-1}^{(1)},\overline{a}_{-1}^{(2)},...,\overline{a}_{-1}^{(n)}\right\}$, $\left\{a_k^{(1)},a_k^{(2)},...,a_k^{(n)}\right\}$, $\left\{\overline{a}_{-(k-2)}^{(1)},\overline{a}_{-(k-2)}^{(2)},...,\overline{a}_{-(k-2)}^{(n)}\right\}$, $\left\{b_0^{(2)},b_0^{(3)},...,b_0^{(n)}\right\}$, $\left\{b_1^{(1)},b_1^{(2)},...,b_1^{(n)}\right\}$, $\left\{\overline{b}_{-1}^{(1)},\overline{b}_{-1}^{(2)},...,\overline{b}_{-1}^{(n)}\right\}$, $\left\{\overline{b}_{-2}^{(1)},\overline{b}_{-2}^{(2)},...,\overline{b}_{-2}^{(n)}\right\}$, $\left\{\overline{b}_{-3}^{(1)},\overline{b}_{-3}^{(2)},...,\overline{b}_{-3}^{(n)}\right\}$, $\left\{b_{k-2}^{(1)},b_{k-2}^{(2)},...,b_{k-2}^{(n)}\right\}$ and $\left\{\overline{b}_{-k}^{(1)},\overline{b}_{-k}^{(2)},...,\overline{b}_{-k}^{(n)}\right\}$, there, indeed, exists a number of $13n-1$ equations, as expected and thus the problem has a solution. In other words, Eqs.(15), (16), (17) and (18) comprise $2n$, $3n-1$, $4n$ and $4n$ equations, respectively, i.e., a total sum of $13n-1$. Thus, $a_k^{(j)}$ and $b_k^{(j)}$ are indeed obtainable from Eqs.(15-18), and in this context $\varphi_j(z)$ and $\psi_j(z)$ can be recapitulated as follows:

$$\varphi_j(z) = \alpha_1^{(j)}z + a_3^{(j)}z^3 + \sum_{k=5,7,9,...} a_k^{(j)}z^k + a_{-1}^{(j)}z^{-1} + \sum_{k=5,7,9,...} a_{-(k-2)}^{(j)}z^{-(k-2)}, \quad \big(j = 1,2,...,n\big) \qquad (19)$$

$$\psi_j(z) = b_1^{(j)}z + \sum_{k=5,7,9,...} b_{k-2}^{(j)}z^{k-2} + b_{-1}^{(j)}z^{-1} + b_{-3}^{(j)}z^{-3} + \sum_{k=5,7,9,...} b_{-k}^{(j)}z^{-k}, \qquad (j=1,2,...,n) \qquad (20)$$

where 'even' terms are missing since are all zero.

Before concluding it should be mentioned that:

(a) by setting $p_I=0$ in the first of Eqs.(15), the present formulae [Eqs.(15-20)] provide the solution in case internal uniform pressure is zero and the multi-layered ring is only under the action of external uniform pressure p_E and external parabolic pressure $p(\theta)$ (along two finite arcs of its outer periphery, antisymmetric with respect to x-axis),

(b) by setting $p_E=0$ in the second of Eqs.(15), the present formulae [Eqs.(15-20)] provide the solution in case external uniform pressure is zero and the multi-layered ring is only under the action of internal uniform pressure p_I and external parabolic pressure $p(\theta)$,

(c) by setting $p_I=0$ in the first of Eqs.(15) and $p_E=0$ in the second of Eqs.(15), the present formulae [Eqs.(15-20)] provide the solution in the case the multi-layered ring is only under the action of external parabolic pressure $p(\theta)$,

(d) by setting $P_c=0$ in Eqs.(15, 17 and 18), the present formulae [Eqs.(15-20)] provide the solution in the case external parabolic pressure is zero and the multi-layered ring is only under the action of internal uniform pressure p_I and external uniform pressure p_E,

(e) by setting $P_c=0$ in Eqs.(15, 17 and 18) and $p_I=0$ in the first of Eqs.(15), the present formulae [Eqs.(15-20)] provide the solution in the case internal uniform and external parabolic pressure are zero and the multi-layered ring is only under the action of externally imposed pressure p_E and

(f) by setting $P_c=0$ in Eqs.(15, 17 and 18) and $p_E=0$ in the second of Eqs.(15), the present formulae [Eqs.(15-20)] provide the solution in the case external uniform and parabolic pressure are zero and the multi-layered ring is only under the action of internal uniform pressure p_I.

Particularly, in all last three cases (d, e, f), i.e., when only uniform pressure over one or both the two boundaries (internal and external) of the multi-layered ring is present, the complex potentials are significantly simplified to:

$$\varphi_j(z) = \alpha_1^{(j)}z, \quad \psi_j(z) = \frac{b_{-1}^{(j)}}{z}, \quad (j=1,2,...,n) \qquad (21)$$

where $\alpha_1^{(j)} \in \mathbb{R}$ and $b_{-1}^{(j)}$ are now just provided by only Eqs.(15), for $P_c = 0$, and for: $p_I \neq 0, p_E \neq 0$ in case (d), $p_I = 0, p_E \neq 0$ in case (e) and $p_I \neq 0, p_E = 0$ in case (f).
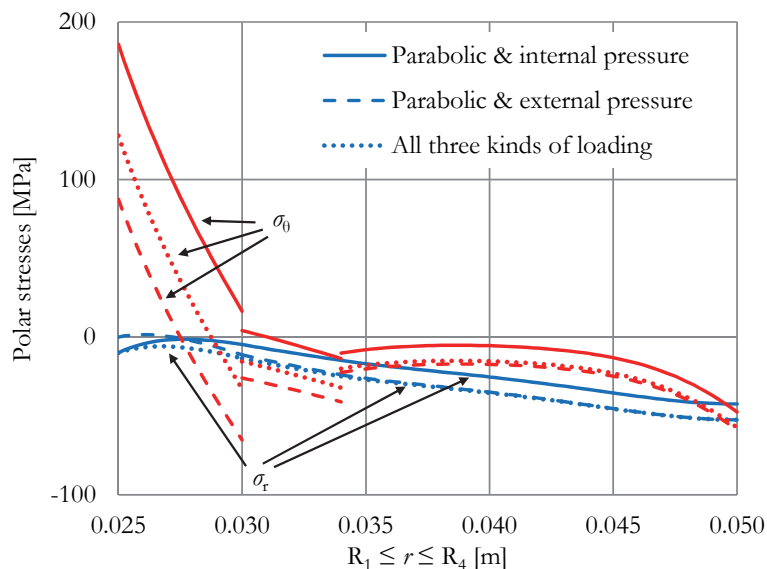

Figure 2: Distribution of stresses along the diameter corresponding to the symmetry axis of the parabolic load, for three loading schemes. Internal pressure=External pressure=10 MPa, P_{frame}=5 kN, ω_o=10°, P_c=43.1 MPa, n=3. Composite ring's thickness w=0.01 m. Inner ring (1): $R_1 \leq r \leq R_2$, R_1=0.025 m, R_2=0.030 m, E_1=30 GPa, ν_1=0.25. Intermediate ring (2): $R_2 \leq r \leq R_3$, R_2=0.030 m, R_3=0.034 m, E_2=10 GPa, ν_2=0.30. Outer ring (3): $R_3 \leq r \leq R_4$, R_3=0.034 m, R_4=0.050 m, E_3=3 GPa, ν_2=0.35).

In order to demonstrate the capabilities of the solution introduced, the distribution of the radial and tangential stresses along the diameter corresponding to the symmetry axis of the parabolic load, is plotted in Fig.2, for three combinations of the constituent loading schemes, i.e., parabolic distribution of radial stresses and uniform internal pressure, parabolic distribution of radial stresses and uniform external pressure, and finally all three schemes simultaneously. The discontinuity of the distribution of transverse stress at the interfaces of the rings is the main characteristic of the plots. As it was expected, this discontinuity is stronger for the case of simultaneous action of the parabolic distribution and external uniform pressure.

NUMERICAL ANALYSIS - APPLICATION FOR n=3 CONSTITUENT RINGS

As a next step, a parametric numerical analysis was decided to be carried out, in order to explore the influence of various factors on the displacement- and stress-fields developed in a multi-layered ring. The ring with three layers under plane strain conditions was decided to be considered, due to its increased practical interest. The principal advantage of the numerical scheme is that it models the "multi-layered ring - jaw" complex (as an integrated elastic system) rather than the isolated ring. Before the main numerical study, the model was properly validated as it is described in next section.

Construction and validation of the reference numerical model
For the proper validation of the numerical model advantage was, initially, taken of the analytic solution for the most complex loading case, i.e., the partial parabolic pressure. For symmetry reasons (materials and geometry) only a quarter of the ring-jaw complex ($0^o \leq \theta \leq 90^o$) was constructed with the aid of ANSYS software. The geometry of the reference model is shown in Fig.3. For the radii of the layers it holds that R_j=25, 30, 34, 50 mm, for $1 \leq j \leq 4$. All three interfaces (i.e., between the constituent rings and between the jaw and the outer ring) were taken into account.
The model was meshed using the PLANE182 element. Contact elements (CONTA172 and TARGE169) were used to model the interfaces. The interfaces between the successive rings were considered as mutually bonded without separation. A very small (tending to zero) value was assigned to the coefficient of friction at the interface between the jaw and the external surface of the outer ring, in order to minimize (eliminate) friction stresses. This assumption was dictated by the fact that the analytic solution, described in the previous section, considers an isolated ring under exclusively radial stresses without any friction stresses at all.
The analysis performed was linearly elastic. The moduli of elasticity and the Poisson's ratios assigned to each one of the rings were E_j=30, 10, 3 GPa and v_j=0.25, 0.30, 0.35, respectively, for $1 \leq j \leq 3$. The jaw was considered to be made of steel (E_{jaw}=210 GPa and v_{jaw}=0.30).
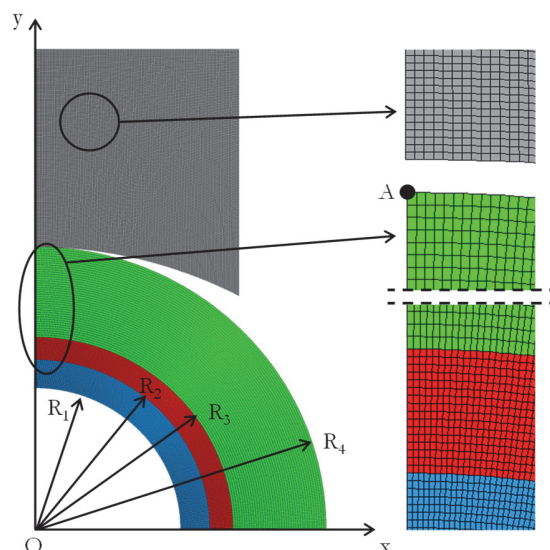

Figure 3: The reference numerical model and detailed views of the finally adopted mesh.

Due to the model's symmetry the following boundary conditions were adopted:
i.   The motion along the *y*-axis (loading axis) of all the nodes of the lower line of the ring was restricted.

ii. All the nodes of the left (vertical) line of the ring as well as the nodes of both sides of the jaw were restricted of shifting horizontally (i.e., normally to the loading axis).

iii. A uniform vertical displacement on the nodes of the upper line of the jaw was imposed.

The optimum element size for the meshing of the model was chosen based on a proper convergence analysis. The variation of the polar stresses developed along "Path 0", i.e., the outer periphery of the outermost ring, and especially around the position where the major differences are observed is plotted in Fig.4a. The embedded graph corresponds to the stresses along the whole length of "Path 0". In addition, the total stress applied on point A (see Fig.3) is plotted in Fig.4b. Both graphs indicate that convergence is satisfactory for about 20000 elements. In order to obtain more accurate results (and given that the CPU-time consumption is not prohibitive), a number of about 38000 elements was chosen for the final meshing.
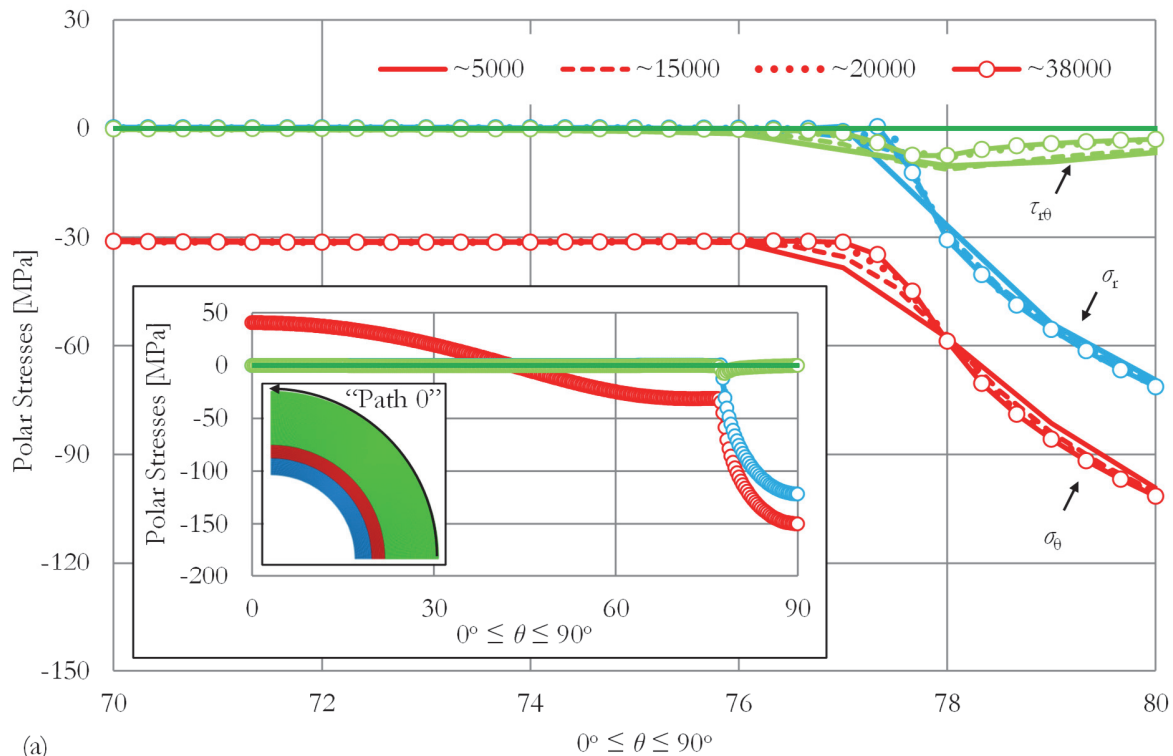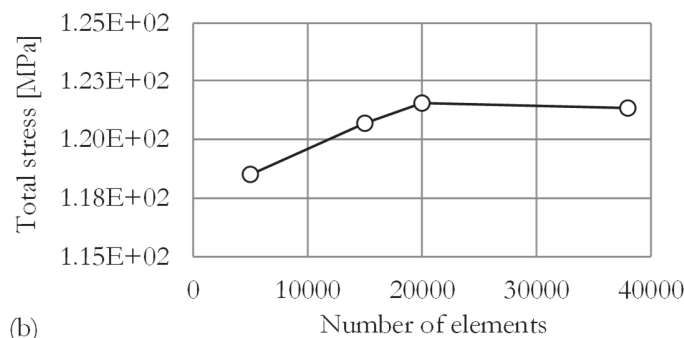
Figure 4: (a) The variation of the polar stresses developed along "Path 0" (the embedded graph corresponds to the whole length of "Path 0") and (b) the total stress applied on point A (see Fig.3) for various numbers of elements.

Before proceeding to the parametric study, the numerical model was used to check the assumption of the analytic solution concerning the parabolic distribution of radial stresses along the loaded arc of the ring. This was considered absolutely necessary because the specific assumption is based on the solution of a different problem, i.e., that of the "*compact* disc - jaw" contact problem [5] and therefore adopting a similar distribution for the "*ring* - jaw" problem appears perhaps somehow arbitrary. In this context, the vertical displacement of the upper node (point A in Fig.3) of the ring (which is, in fact, the only point of the ring in contact with the jaw before the onset of loading) was determined according to the analytic

solution described in previous section, assuming now that ω_o is not arbitrarily prescribed (as it was considered in Eqs.(1)), but it is rather provided, together with P_o, by the relevant compact disc-jaw contact problem [5].Then a uniform displacement was applied at the steel jaw (simulating in fact the load exerted by the loading frame during the laboratory experiments with the device suggested by ISRM for the standardized Brazilian-disc test), the magnitude of which was determined by demanding that it should result to a vertical displacement of point A equal to the respective one provided by the analytic solution. The results of the numerical analysis for the distribution of pressure along the common contact arc, developed at the ring-jaw interface are plotted in Fig.5, in conjunction with the parabolic pressure applied on the ring during the theoretical solution. It is seen from this figure that the two distributions are in relatively good agreement, despite some differences concerning their amplitude (equal to about 140 MPa for the analytic solution and 122 MPa for the numerical one) and also their flatness (the numerically obtained distribution appears somehow flatter). These differences should be expected, given that the parabolic distribution is an approximation of the actual "cyclic" distribution [5, 6] (developed during the contact of two elastic cylindrical bodies), which was adopted in an attempt to achieve closed-form analytic expressions for the distribution of stresses a displacements all over the disc [7, 8]. (It is here recalled, that for the actual "cyclic" distribution analytic expressions for the stress field cannot be straightforwardly obtained [5]).
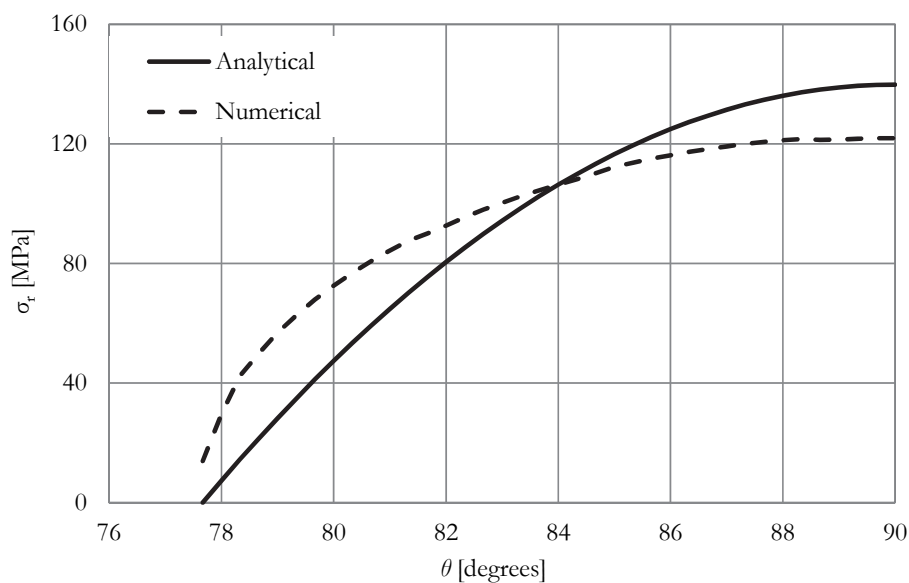

Figure 5: The applied pressure applied on the ring based on both the analytical and the numerical analysis.

Besides the above mentioned slight differences, it is quite astonishing that the analytic and the numerical approaches provide almost identical results for the "total" pressure applied on the ring indicating the static equivalency of the two solutions. Even more astonishing is the fact that the length of the contact arcs obtained by the two solutions (numerical and analytic) is again almost identical: The contact arc $2\omega_o$ determined from the numerical model equals to 24.67° while the respective one of the analytical solution is equal to 24.59°. The same excellent agreement was observed, also, for the variation of displacements and stresses along strategic paths of the model, as it can be seen, for example, in Fig.6, in which analytical versus numerical results concerning the vertical displacement (Fig.6a) and the polar stresses (Fig.6b) are plotted for "Path 1", i.e., along the diameter corresponding to the axis of loading symmetry. The differences observed are quite marginal. For example, for the displacements, the difference does not exceed 4% (Fig.6a) while for the polar stresses the differences are almost tending to zero (Fig.6b).

As an additional validation step, results of the numerical analysis were compared against the respective ones analytically obtained, also, for some combinations of the three loading schemes considered (parabolic pressure, external uniform pressure and internal uniform pressure). For this specific step the jaw was removed and the multi-layered ring was modeled as an isolated elastic body (for convenience). The following loading schemes were imposed on the ring:

Case 1: Pressure was applied on the nodes of the outer perimeter of the outermost ring along a contact length $2\omega_o$ which was assumed equal to 20°. The parabolic pressure variation corresponds to a statically equivalent force equal to 5 kN applied by the loading frame.

Case 2: Internal pressure equal to 10 MPa was applied on all nodes along the inner perimeter of the three-layered ring.

Case 3: External pressure equal to 10 MPa was applied on all nodes along the outer perimeter of the three-layered ring.

Case 4: Combination of Cases 1 and 2.
Case 5: Combination of Cases 1 and 3.
Case 6: All three types of loading, i.e., combination of Cases 1, 2, 3.

The normal polar stresses (both radial and transverse) obtained by the numerical model for all six loading cases mentioned above are presented in Fig.7 in juxtaposition to the respective analytical results. The plots are realized, as in Fig.6, along the diameter corresponding to the symmetry axis of the loading distribution. It is clear that the correlation between analytic and numerical results is quite satisfactory, for both stresses and for all loading schemes without any exception.
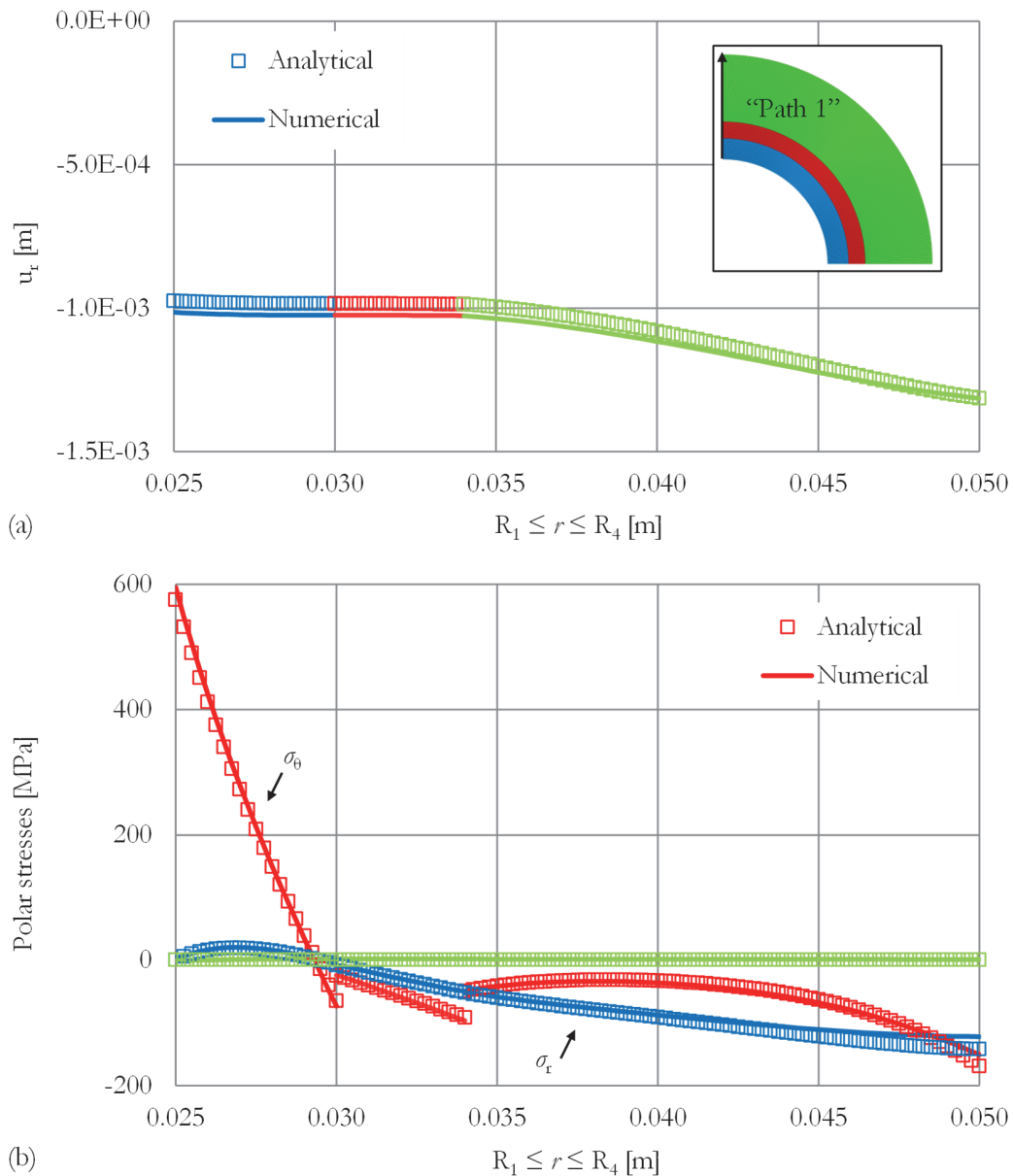

Figure 6: Analytical vs. numerical results for the (a) vertical displacement and (b) the polar stresses developed along "Path 1".

Recapitulating the data of the validation procedure, it can be definitely concluded that the numerical model approaches the analytic solution in an excellent manner. Therefore, it is safe for the model to be used for a thorough parametric analysis of the role of the (quite a few) factors, which are expected to crucially affect the overall mechanical response of the multi-layered ring, in case it is subjected to various combinations of the three constituent loading schemes considered (internal and external pressure and parabolic variation of radial stresses). Moreover, the results of the present section, besides validating the numerical model, indicated that the actual stress distribution along the contact arc at the ring-jaw interface is

rather insensitive to whether the disc squeezed between the ISRM jaws is compact or hollow, i.e., ring (either it is homogeneous or it consists of successive layers with different mechanical properties), at least for low to moderate values of the externally applied load and provided relatively thick-walled rings are considered.
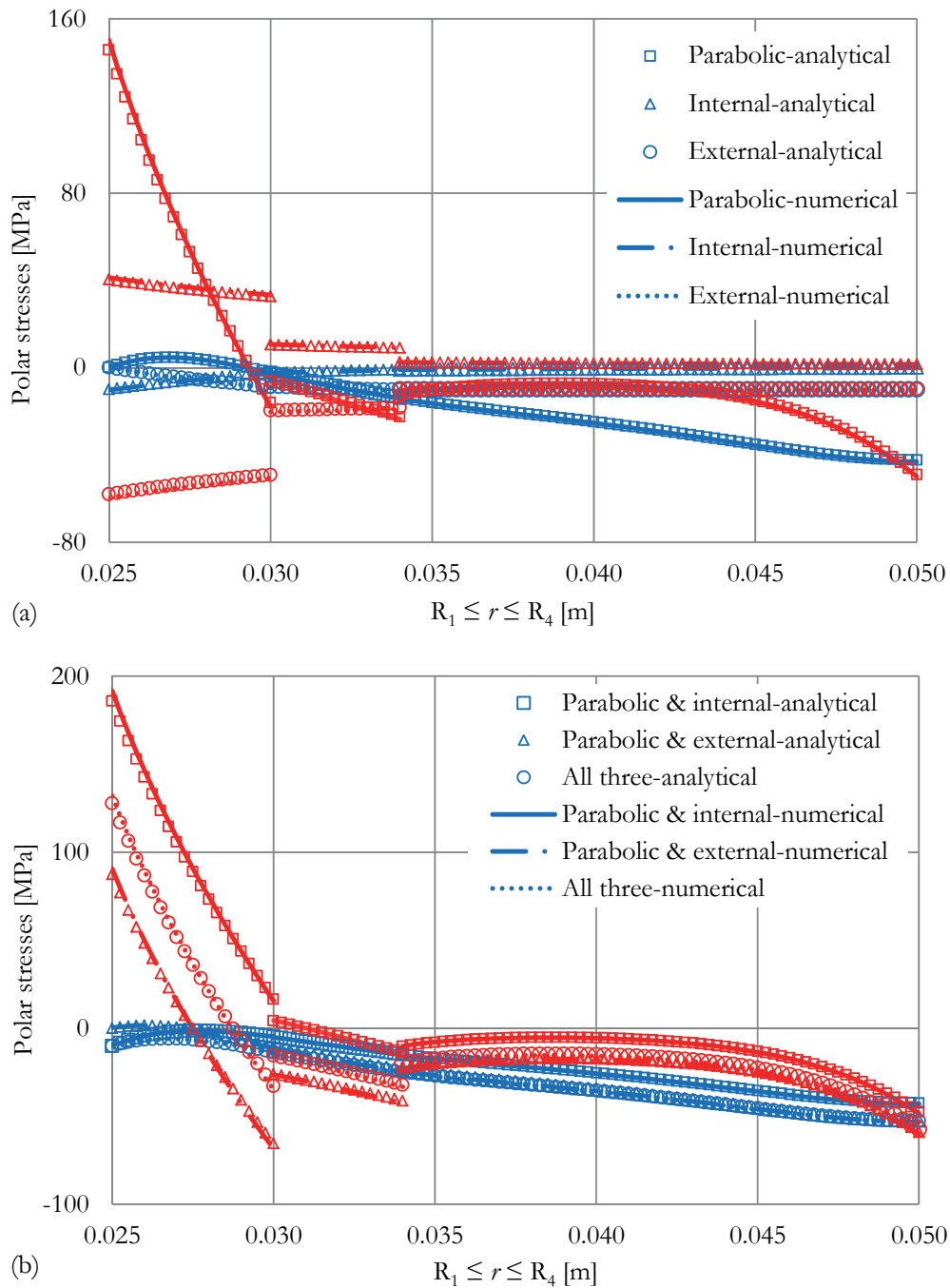

Figure 7: Analytical vs. numerical results for (a) simple and (b) complex loading schemes. Blue lines correspond to radial stress while red ones correspond to transverse stress.

Parametric numerical analysis

The as above exhaustively validated numerical model is now used for a parametric analysis. In this direction, a series of new models was constructed for the most complicated loading constituent, i.e., the parabolic pressure. Three parameters were taken into account in the present study, the influence of which is expected to be more crucial. These parameters are:

a. The modulus of elasticity of the intermediate ring, E_2.
b. The thickness of the intermediate ring, $t_2=R_3-R_2$, keeping the ring's outer diameter constant, i.e., increasing t_2 results to decrease of the thickness of the outermost ring, $t_3=R_4-R_3$.
c. The contact length, or equivalently the length of the loaded arc, $2\omega_o$, assuming that the overall externally imposed load is kept constant. In this case the jaw was not taken into account. Concerning the distribution of the pressure applied along each contact arc, it was determined by taking advantage of Eqs.(1).

The numerical values assigned to each one of the three parameters studied are summarized in Tab. 1. In addition, the variation of the applied pressure for the values considered for the length of the half contact arc ω_o is plotted in Fig.8. As it is expected, by decreasing the length of the loaded arc (while keeping the overall load constant) the amplitude of the distribution increases, leading to increased stress concentration in the immediate vicinity of the loaded arc, which in turn increases the possibility for premature failure in this region of the ring. This aspect should be carefully taken into account in case the external layer of the ring is made of relatively brittle materials.

Parameter	Values					
E_2 [GPa]	5.0	7.5	12.5	15.0	17.5	20.0
t_2 [mm]	1	2	3	5	6	
ω_o [deg]	1	3	5	7	9	11

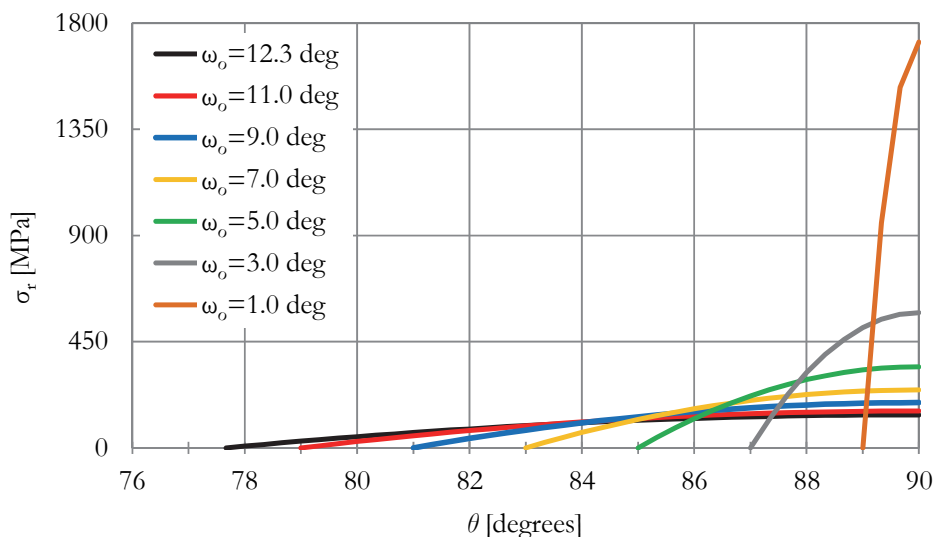Table 1: The numerical values assigned to each parameter.

Figure 8: The variation of the pressure applied on the ring for various ω_o-values.

RESULTS AND DISCUSSION

The influence of the elastic modulus of the intermediate ring, E_2

The displacement along the loading axis (i.e., *y*-axis) developed all over the ring's area is presented in Fig.9a for the reference model. Its variation along *y*-axis for various E_2 values is exhibited in Fig.9b. It is interesting to observe that, although the values of E_2 vary within a relatively wide range (from -50% to +100% of the respective value of the reference model), the displacements along *y*-axis are more or less insensitive to this variation. The maximum difference does not exceed 3% and it is observed for E_2=20 GPa.

On the contrary, the stresses developed in the ring are much more sensitive to the changes of E_2. To enlighten this point (and considering that the polar reference system is much more convenient for the specific application), the variation of the transverse stress (σ_θ) along the loaded diameter is plotted in Fig.10 for all E_2 values studied. It is seen that the influence of E_2 is very strong, especially at the interface points between the constituent rings. As it is perhaps expected, the "stress jump"

is amplified as the difference of the modulus of elasticity of ring 2 from the elastic modulus of the adjacent ring increases. Therefore, the variation of σ_θ from ring 1 (innermost) to ring 2 (intermediate) is smoother when E_2=20 GPa while from ring 2 to ring 3 (outermost) the variation is smoother when E_2=5 GPa. It is also noted that σ_θ is negative all along rings 2, 3 (along the specific path) for all E_2 values studied, while it changes sign somewhere along ring 1.

The variation of the polar stresses developed along the interfaces is quite interesting. For the interface between rings 1, 2 and more specifically along the outer periphery of ring 1 (Fig.11a), σ_θ is affected more severely. When the value of E_2 is between the elastic moduli of the two surrounding rings, the variation of σ_θ is again very smooth with small variations. For E_2<10 GPa the transverse stress becomes larger as θ increases while the opposite is true for E_2>10 GPa. It is also seen from the same figure that the values of $\sigma_{r\theta}$ developed along the interface are of the same order of magnitude with σ_θ.
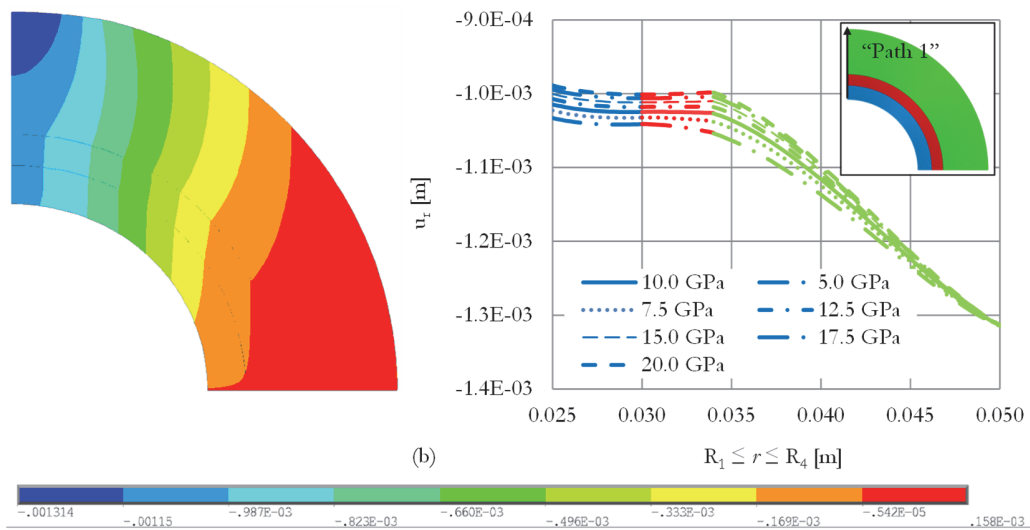

Figure 9: (a) The distribution of the u_y component of the displacement field in [m]. (b) The variation of u_y along "Path 1" for various values of the elastic modulus of the intermediate ring (E_2). The colours of the lines of the graph are in agreement to the colour code of the embedded figure.
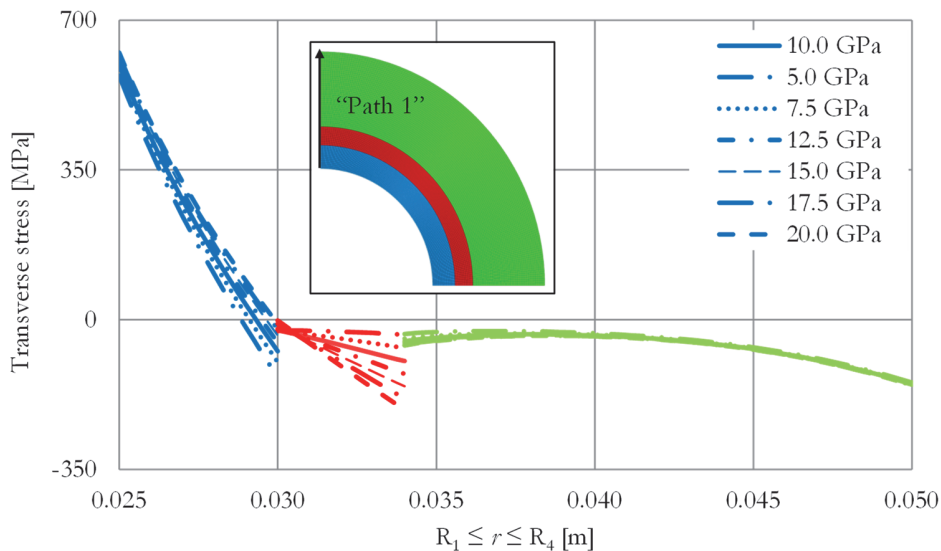

Figure 10: The transverse stress along "Path 1" for various values of the elastic modules, E_2, of the intermediate ring. The colours of the lines of the graph are in agreement to the colour code of the embedded figure.

As the modulus of elasticity of ring 2 increases, $\sigma_{r\theta}$ also increases, attaining its maximum value when $\theta \sim 65°$. The radial stress also attains its maximum value when θ is equal to about 65°, although a slight "move" to a lower value of θ is observed as E_2 increases. It is also to be noted that the changes of σ_r are not significant all along the outer periphery of ring 1.

The variation of stresses along the inner periphery of ring 3 (interface between rings 2 and 3) is plotted in Fig.11b. It is clear that the variation of both radial and shear stresses is qualitatively similar to the respective one along the outer periphery of ring 1 but their magnitudes are lower. The radial stress attains its maximum value when θ is equal to about 60° and the differences are mainly detected when θ varies from about 75° to 90°. Concerning the shear stress, it attains its maximum value when $\theta \sim 70°$. In addition, it seems that the exact position of the maximum shear stress "moves" slightly to larger θ values with increasing E_2. On the other hand, the variation of the transverse stress is monotonous all along the specific path, contrary to what it was observed along the outer periphery of ring 1.
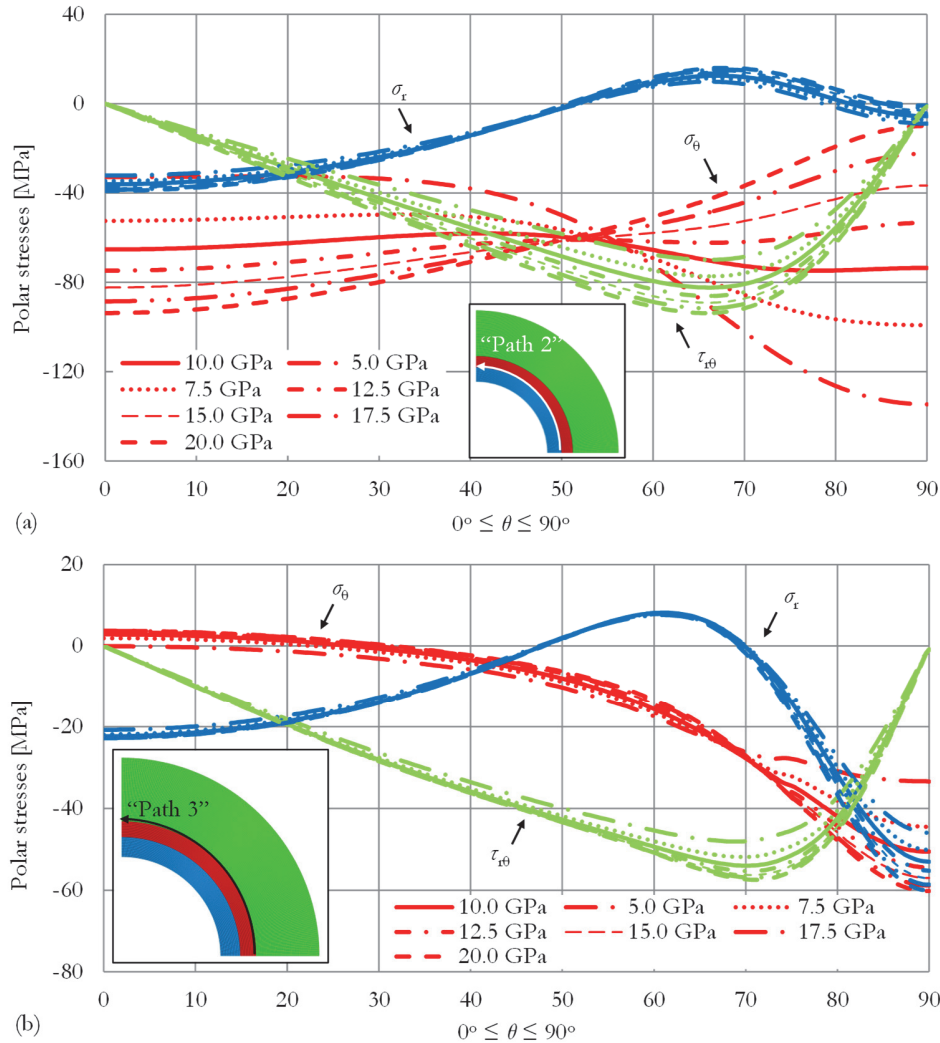

Figure 11: (a) The variation of the polar stresses along "Path 2" (outer periphery of the innermost ring) for various E_2-values. (b) The variation of the polar stresses along "Path 3" (inner periphery of the outermost ring) for various E_2-values.

The influence of the thickness of the intermediate ring, t_2

The effect of the thickness of the intermediate ring on the variation of stresses along the outer periphery of ring 1 (Fig.12a) is very similar to the one presented in Fig.11a (where the parameter studied was the modulus of elasticity of ring 2) both qualitatively and quantitatively. For t_2=4 mm (reference model) the variation of σ_θ is again smoother. For t_2<4 mm σ_θ increases with increasing θ while for t_2>4 mm σ_θ increases with decreasing θ. The shear stress, on the other hand, increases continuously with increasing t_2 and its maximum value is again detected around $\theta \sim 65°$ independently of the values of t_2 considered here. Increase of t_2 leads also to increase of the radial stress developed. Again its maximum value seems to "move" slightly towards larger θ-value as t_2 increases.

The variation of stresses along the inner periphery of ring 3 is exhibited in Fig.12b and it is similar to the respective one in Fig.11b. However, and despite this qualitative similarity, the thickness of the intermediate ring affects more the stress field along the inner periphery of the outermost ring 3. The differences are generally larger, especially around θ=0° and θ=90°. This is true for both radial and transverse stresses. On the contrary, the shear stress attains its maximum value at θ~65° when t_2=1 mm while as t_2 increases the maximum shear stress appears at slightly larger values of θ.
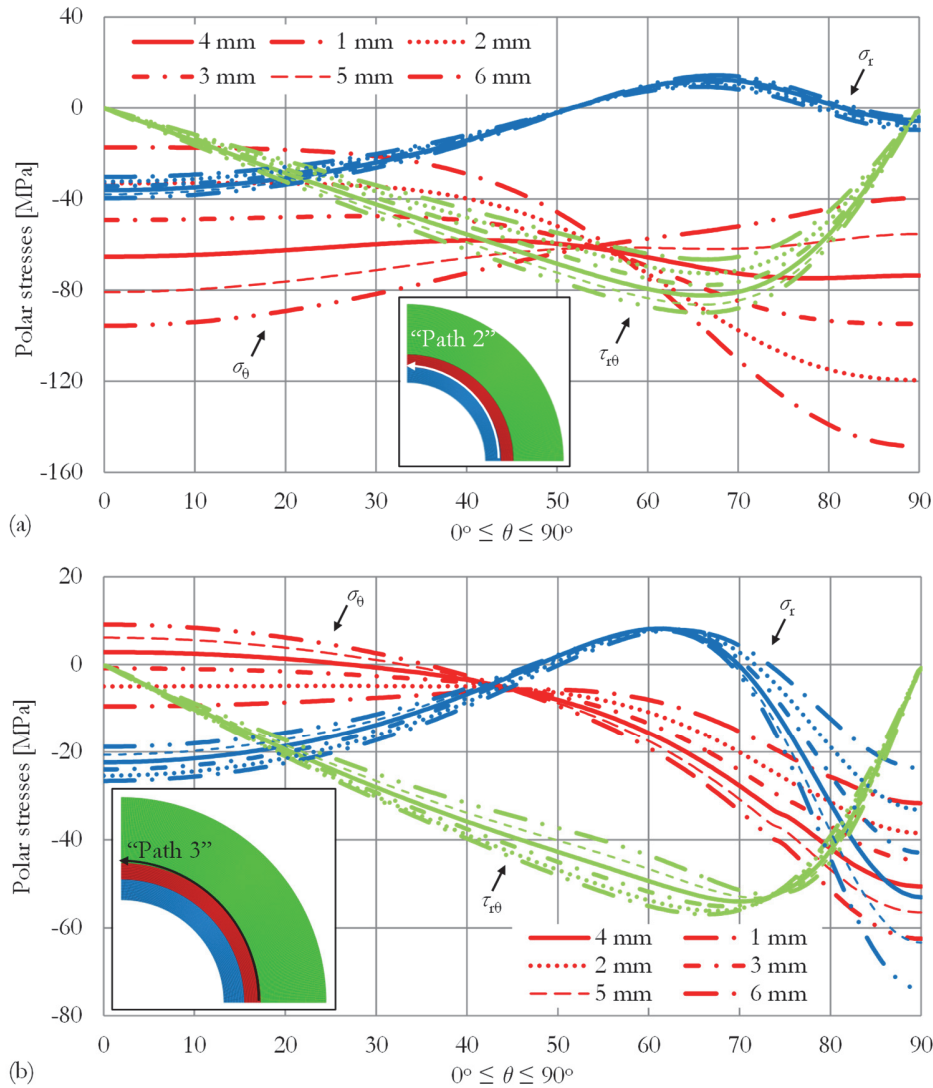

Figure 12: The variation of the polar stresses developed along (a) "Path 2" - outer periphery of innermost ring and (b) "Path 3" - inner periphery of outermost ring for various values assigned to the thickness of the intermediate ring (t_2).

Another interesting point is that the contact length between the outermost ring and the jaw, as well as the pressure applied along it, are only slightly influenced by the thickness of the intermediate ring, as it can be seen in Fig.13. The lower t_2 is, the smaller the contact length is (i.e., for t_2=1 mm, $2\omega_o$=23.34° while for t_2=6 mm, $2\omega_o$=24.67°) and the lower the maximum pressure applied on the ring is (keeping the externally applied displacement on the jaw constant).

The role of the contact length, $2\omega_o$
Keeping the "total" pressure applied constant and at the same time narrowing the contact length ω_o, results to interesting changes of the polar stresses developed along the interfaces. It is recalled here that the specific parameter is studied for an isolated ring rather than the ring-jaw complex. Therefore the contact length for the reference model is here set equal to that obtained during the validation procedure, which was equal to $2\omega_o$=24.60°.
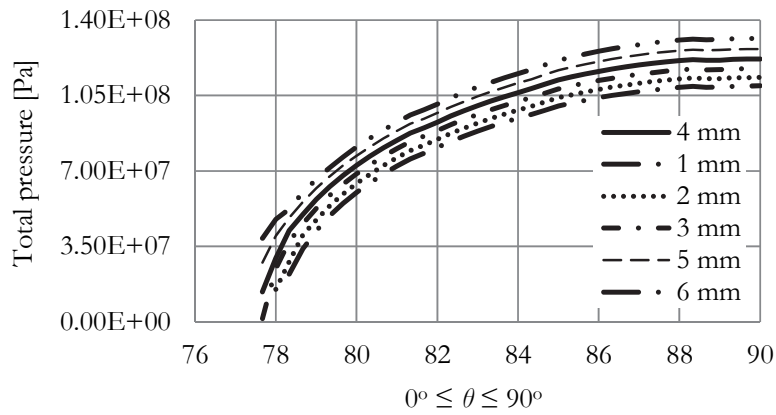
Figure 13: The variation of the total pressure applied on the ring for various t_2-values.
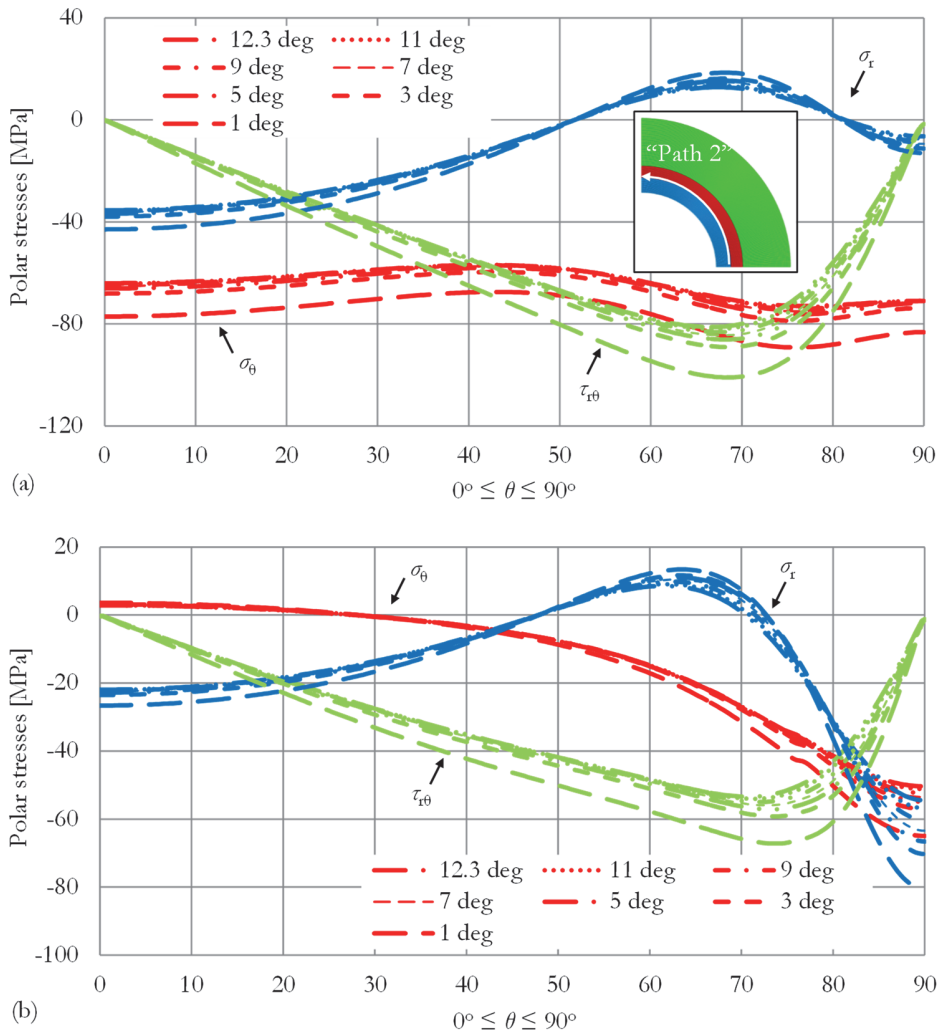

Figure 14: The variation of the polar stresses developed along (a) "Path 2" - outer periphery of innermost ring and (b) "Path 3" - inner periphery of outermost ring for various values assigned to the half contact length (ω_o).

Indeed, along the outer periphery of ring 1 (Fig.14a) the transverse stress σ_θ seems to be almost independent of the contact length for $\omega_o \geq 5^o$. The changes are noticeable only for $\omega_o < 5^o$ and the respective variations are almost similar to the aforementioned ones (attaining of course larger values). The same is more or less true concerning the shear stress. As the contact length becomes narrower, the shear stress increases (the changes are larger as ω_o decreases) attaining its maximum value at about $\theta \sim 70^o$. Similar conclusions are drawn, also, for the variation of the radial stresses.

The variation of the transverse stress σ_θ along the inner periphery of ring 3 is exhibited in Fig.14b. As ω_o decreases the changes of σ_θ are more pronounced and the maximum difference recorded is equal to about 15% for $\omega_o=3^o$ (in comparison to the reference model for which $\omega_o=12.33^o$). In case $\omega_o=1^o$, almost half of the periphery is affected and the difference now reaches about 30%. The radial stress is also strongly affected, reaching 50% larger value at $\theta=90^o$ when $\omega_o=1°$ compared to the respective stress when $\omega_o=12.33^o$. Concerning the shear stress, it is again larger as ω_o decreases attaining its maximum value around $\theta=70^o$.

CONCLUSIONS

An analytic solution for the mechanical response of a multi-layered ring under a combined loading scheme, including both uniform internal and external pressure and also parabolic distribution of radial stresses along two finite arcs of its external periphery was introduced. The solution was obtained in series form with the aid of Savin's pioneering approach for the infinite plate with a hole strengthened by rings. The main advantage of the analytic procedure described is that it is capable of providing the full-field stress- and displacement-fields for any combination of the three constituent loading schemes considered. As an application the three-layered ring was studied due to its increased practical importance.

In order for a closed form full-field solution to be achieved, some critical assumptions were adopted, besides the familiar ones related to the linearity, homogeneity and isotropy of the ring's constituent materials. These assumptions are related to the ideal bonding between the ring's successive layers, the absence of any kind of friction and the distribution of radial stresses along the loaded arcs, which was considered of parabolic nature, in accordance with the respective distribution for an intact disc compressed between the jaws suggested by ISRM for the implementation of the Brazilian-disc test.

The analytic solution was used to validate a flexible numerical model, in the direction of implementing thorough parametric studies. The advantage of the numerical model was the fact that it considered the ring and the jaw as a system of elastic bodies in equilibrium, approaching experimental reality in a much more accurate manner. The model was exhaustively validated taking advantage of the analytic results. During the validation process it was concluded that the actual stress distribution along the contact arc at the ring-jaw interface is more or less independent of some crucial geometric characteristics. In fact, it was proven that the specific distribution in case the body compressed between the ISRM jaws is intact (disc) does not exhibit significant differences compared to the respective distribution for a body weakened by the presence of a circular hole (irrespectively of whether it is a homogeneous ring or a ring consisting of successive layers with different mechanical properties). In general, the assumptions adopted during the formulation of the analytic problem for the loading scheme of the isolated ring were in excellent agreement with the conditions along the ring-jaw contact arc obtained by the numerical study of the ring-jaw complex.

The parametric study revealed quite a few interesting aspects concerning the influence of three critical parameters on the stress- and displacement-fields developed in the multi-layered ring. Generally speaking, this influence is of complicated, non-monotonous nature, rendering further parametric analysis with simultaneous variation of these parameters unavoidable.

REFERENCES

[1] Markides, Ch.F, Pasiou, E.D., Kourkoulis, S.K., The multi-layered ring under parabolic pressure, Engineering Transactions, 64(4) (2016) 433-440.
[2] ISRM, Suggested methods for determining tensile strength of rock materials, International Journal of Rock Mechanics and Mining Sciences and Geomechanics Abstracts, 15(3) (1978) 99–103.
[3] Savin, G.N., Stress concentration around holes, Pergamon Press, Oxford (1961).
[4] Muskhelishvili, N.I., Some basic problems of the mathematical theory of elasticity, 4th edition, P. Noordhoff Groningen, The Netherlands (1963).
[5] Kourkoulis, S.K., Markides, Ch.F., Chatzistergos, P.E., The standardized Brazilian disc test as a contact problem, International Journal of Rock Mechanics and Mining Sciences, 57 (2012) 132-141.

[6] Timoshenko, S.P., Goodier, J.N., Theory of elasticity, McGraw-Hill, New York (1970).

[7] Markides, Ch.F., Kourkoulis, S.K., The stress field in a standardized Brazilian disc: The influence of the loading type acting on the actual contact length, Rock Mechanics and Rock Engineering, 45(2) (2012) 145-158.

[8] Kourkoulis, S.K., Markides, Ch.F., Chatzistergos, P.E., The Brazilian disc under parabolically varying load: Theoretical and experimental study of the displacement field, International Journal of Solids and Structures, 49(7-8) (2012) 959-972.